Field Effect Transport Measurements on Single Grains of Sexithiophene: Role of the Contacts

ARTICLE *in* THE JOURNAL OF PHYSICAL CHEMISTRY B · NOVEMBER 2000

Impact Factor: 3.3 · DOI: 10.1021/jp002782o

Field Effect Transport Measurements on Single Grains of Sexithiophene: Role of the Contacts

Anna B. Chwang and C. Daniel Frisbie*

Department of Chemical Engineering and Materials Science, University of Minnesota, 421 Washington Avenue SE, Minneapolis, Minnesota 55455

Received: August 2, 2000; In Final Form: October 2, 2000

This paper presents a study of the contact properties of field effect transistors (FETs) based on single grains of the organic semiconductor sexithiophene ('6T', $E_{gap} \sim 2.3$ eV). The FETs are constructed by vapor deposition of isolated 6T grains 2−15 nm thick and 1−3 μm wide into <500 nm gaps between Au wires pre-patterned on SiO_2/Si substrates. The Au wires serve as source and drain contacts to the grain and the doped Si substrate serves as the gate electrode. We show from the contact area dependence of the drain current−drain voltage characteristics that the FETs are contact limited. Both the source/6T and drain/6T interfaces can be considered to be Schottky contacts and, consequently, the device can be modeled as a pair of back-to-back diodes. Current is limited by the reverse-biased, hole injecting source/6T contact where the mechanism of hole injection from the metal to the semiconductor is best described by a drift/diffusion process with a field-dependent mobility. The contact resistance of the source/6T interface can be as high as ∼1 GΩ, or ∼10^5 Ω-cm normalized for contact width, and is gate and drain voltage dependent. Greater contact resistances result when the Au electrodes are modified with self-assembled monolayers of dodecanethiol or when Cr is used instead of Au, resulting in dramatically inhibited charge transport.

Introduction

Film microstructure plays a critical role in the overall performance of organic semiconductor-based devices. For example, the dramatic improvement in carrier mobility realized recently in films of the semiconducting oligomers sexithiophene and pentacene is attributed in large part to the propensity of these materials for forming large, well-ordered grains when vapor deposited.[1] Recent work on organic field effect transistors (OFETs) has also indicated that grain boundaries (GBs) are an important bottleneck to carrier transport.[2] However, the specific effects of GBs in organic semiconductor films (e.g., whether they trap carriers as well as scatter them) are not clear.

Understanding of the role of microstructure on transport can be facilitated by microscopic conductance measurements on *individual* grains and grain boundaries (GBs). Toward this goal, we previously reported an approach for electrically contacting single grains of the organic semiconductor sexithiophene ('6T', $E_{gap} \sim 2.3$ eV).[3]

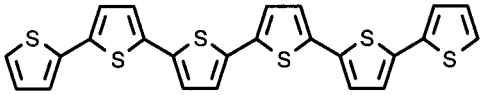

Sexithiophene, 6T

Isolated 6T grains, ∼1 μm in length and width and 2−15 nm thick, were grown by vapor deposition onto an SiO_2/Si substrate pre-patterned with closely spaced pairs of Au wires. Grains that connected pairs of wires were electrically characterized as a function of transverse gate field by applying voltages, as shown in Chart 1A. The structure in Chart 1A constitutes a single-grain field effect transistor (FET) in which the Au wires serve as source and drain electrodes and the doped Si substrate as a gate. In principle, the gate-dependent source-to-drain current (I_D) versus drain voltage (V_D) characteristics allow determination of the carrier mobility, an intrinsic figure of merit. However, the mobility we obtained for single-grain FETs was on the order

CHART 1: (A) Transistor cross-section depicting a 6T grain between two (S and D) electrodes. The 6T is typically 2−14 nm tall, the source (S) and drain (D) electrodes are 15−20 nm tall, and the SiO_2 is ∼150 nm thick. (B) Circuit element depicting the electrode/6T junction diodes and 6T grain resistance. The 6T resistance is negligible compared with the junction resistance. (C) Schematic diagram (top view) illustrating the disordered regions of 6T around the contacts.

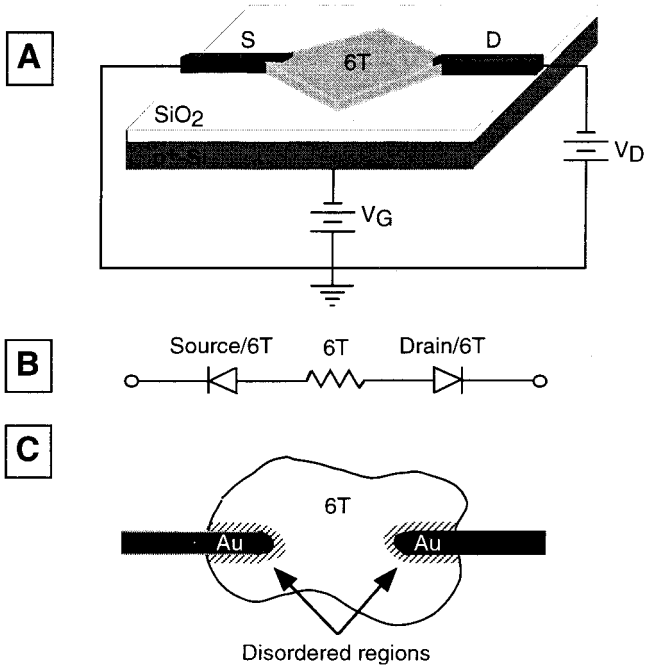

10.1021/jp002782o CCC: $19.00
Published on Web 11/30/2000

of 10^{-4} cm^2/Vs, a low value compared with the highest reported mobility values for 6T FETs.[4] Consequently, we suspected that there was a substantial resistance associated with the Au/6T contacts that depressed the mobility value extracted from the I_D-V_D characteristics. Exploitation of single-grain and multi-grain FETs in future studies to examine the transport properties of GBs required that we elucidate the properties of the Au/6T contacts.

The objective of this study is to show that the I_D-V_D characteristics of the 6T single-grain FETs are dominated by the properties of the source (or hole injecting) contact. To a first approximation, both the source/6T and drain/6T junctions can be considered to be Schottky contacts so that our single-grain FETs are better described as a pair of back-to-back, gate-modulated diodes (Chart 1B). Because 6T behaves as a p-type semiconductor on SiO_2, a negative voltage on the drain results in a forward biased drain/6T junction and a reverse-biased source/6T junction. The resistance of the device is determined by the reverse-biased source/6T contact. Consequently, the observed dependence of I_D on the gate field is due to modulation of the source contact behavior *and not modulation of the 6T grain resistance* as might be supposed based on analogy to standard thin film FETs.

The general form of the Schottky diode equation is[5]

$$J = J_o\left[\exp\left(\frac{qV}{kT}\right) - 1\right] \quad (1)$$

where J is the current density in [A/cm^2], J_o represents the reverse saturation current (metal to semiconductor), and V is the applied bias. For reverse biases $|V| > (3kT/q)$, J is approximately equal to J_o. Because transport in our FETs is dominated by the reversed-biased (source) contact, we are interested in models for J_o. The expression for J_o depends on the relevant transport mechanism. Transport is typically limited by either thermionic emission of carriers over the barrier ϕ_B or subsequent drift/diffusion of carriers in the depletion region (Chart 2A). The term J_o is generally described by the thermionic emission or the drift/diffusion model as:[5]

$$\text{Thermionic Emission:} \quad J_o = qN_v v_r \exp\left(\frac{-\phi_B}{kT}\right) \quad (2A)$$

$$\text{Drift/Diffusion:} \quad J_o = qN_v v_d \exp\left(\frac{-\phi_B}{kT}\right) \quad (2B)$$

where q is the elementary charge, v_r is the recombination velocity of carriers crossing the metal/semiconductor interface, N_v is the effective density of valence band states [for a p-type semiconductor], ϕ_B represents the charge injection barrier in eV, and v_d is the diffusion velocity that, to a first approximation, is equal to the product of the hole mobility, μ, and the electric field across the interface, E ($v_d = \mu E$). For Au/6T contacts, a small barrier ϕ_B to hole injection exists because of the offset between the Fermi level of Au and the valence band or highest occupied molecular orbital (HOMO) of 6T[6] (Chart 2B).

The preexponential term of the drift/diffusion expression for J_o includes an explicit dependence on the interfacial field E ($v_d = \mu E$) that is not present in the thermionic emission model ($v_r \neq v_r(E)$). This difference is because in the drift/diffusion model, carrier transport through the depletion layer is the limiting step and is a field-driven process. Thermionic emission, on the other hand, does not explicitly depend on field (or voltage), though there can be second-order field-induced barrier lowering effects.

CHART 2: (A) Thermionic emission and drift/diffusion transport mechanisms across a metal/p-type semiconductor contact under reverse bias. E_F = fermi energy of the metal, E_V = valence band energy of the semiconductor, E_{Vac} = vacuum energy level, and ϕ_B = barrier to hole injection (from the metal into the semiconductor). (B) Schematic energy level diagram illustrating the effect of V_G on the hole injecting Au/6T contact. As V_G becomes more negative, the depletion width decreases and the electric field increases.

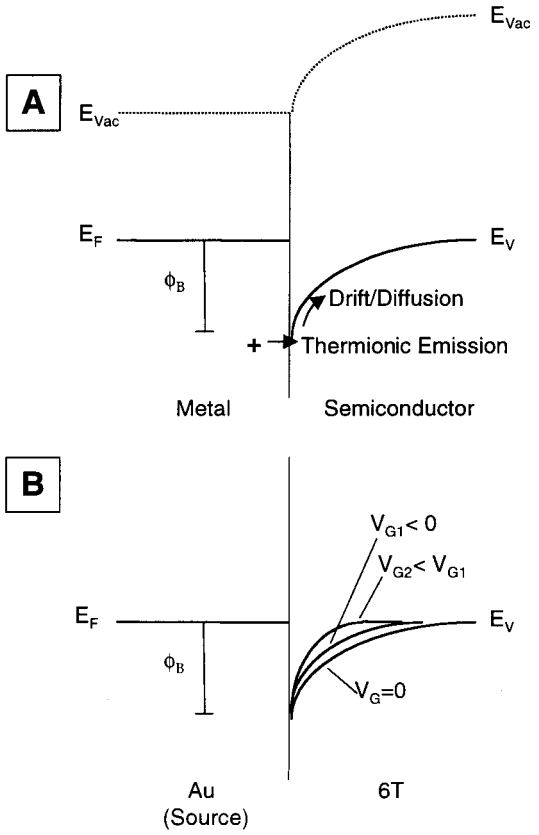

Although thermionic emission more accurately describes charge injection from metals into high mobility semiconductors, drift/diffusion pertains more to injection into low mobility semiconductors.[5] In our devices, there is likely a region of molecular disorder around the Au electrodes due to conformation of the 6T to the irregularly shaped edges of the electrodes (Chart 1C). Because the mobility of a charge carrier in any disordered material is typically low, in absolute terms and relative to the ordered counterpart, we expect drift/diffusion to be more applicable than thermionic emission in describing the transport behavior of our devices. We demonstrate that this is the case in this paper.[7]

A few modifications must be made to eq 2B to apply the drift/diffusion expression for J_o to our gated 6T devices. We replace the barrier ϕ_B from eq 2B with $\Phi(V_D,V_G)$, which we define as an effective barrier. The barrier ϕ_B from eq 2B is an intrinsic quantity of the Au/6T interface that does not take into account nonidealities, such as trap states, which exist near the contact because of disorder. We have shown in previous studies that our devices demonstrate reversible trapping of positive charge carriers.[3] Defining the effective barrier Φ to be a function of V_D and V_G allows us to account for *any* changes in the properties of the Au/6T interface (e.g., trapping or barrier lowering), that are sensitive to the interfacial electric field. We note that the ϕ_B in eq 2A is also replaced by a corresponding effective barrier $\Phi(V_D,V_G)$.

We must also extend our expression for E in the drift/diffusion model to include the field dependence on both V_D and V_G (this modification is not relevant to eq 2A because the thermionic emission model does not include an explicit field dependence). We define E_D to be the component of the field from the laterally applied bias V_D: $E_D = V_D/l$, where l is the characteristic length (depletion width) over which the voltage is dropped. The gate voltage V_G also influences the interfacial electric field as indicated in Chart 2B. Making V_G more negative increases the field by increasing the number of holes in the 6T grain, which decreases the depletion width. Empirically, we have estimated that the electric field E has a power law dependence on the gate voltage, so that E is expressed as

$$E = E_D\left[\frac{(V_G - V_T)}{(V_G - V_T)_o}\right]^n \tag{3}$$

where n is an experimentally determined constant and V_T is the threshold voltage, or the gate voltage at which the device just begins to turn on. The quantity $(V_G - V_T)_o$ is a reference $(V_G - V_T)$ at an arbitrarily chosen gate voltage.

The mobility, μ, of eq 2B ($v_d = \mu E$) can be modeled either as constant or field dependent. The field-dependent mobility is expressed as

$$\mu = \mu_o\left(\frac{V_D}{V_{Do}}\right)^m \tag{4}$$

for $V_D > V_{Do}$, where μ_o is the mobility corresponding to V_{Do} and 'm' is a constant.[8] The V_G dependence of the mobility is not included in eq 4 because it is lumped into the V_G term of eq 3 because n is derived empirically.

In summary, our drift/diffusion expression for J_o is:

$$J_o = qN_v\mu E \exp\left(\frac{-\Phi(V_D, V_G)}{kT}\right) \tag{5}$$

$$J_o = qN_v\left\{\mu_o\left(\frac{V_D}{V_{Do}}\right)^m\right\}\left\{E_D\left[\frac{(V_G - V_T)}{(V_G - V_T)_o}\right]^n\right\}\exp\left(\frac{-\Phi(V_D, V_G)}{kT}\right) \tag{6}$$

An Arrhenius plot of J_o, or I_o because $J_o = I_o$/area, yields the effective barrier Φ.[9] The dependence of Φ on V_D and V_G can be determined by constructing Arrhenius plots at several different drain and gate biases. The constants μ_o, m, and V_T serve as adjustable fitting parameters. The exponent n is determined from log−log plots of $(J_o/\exp(-\Phi/kT))$ versus $(V_G - V_T)$.

Using eq 6, we have been able to successfully model the $I-V$ characteristics of our single-grain FETs. The results establish that these devices are essentially contact limited and that large interfacial fields (or voltage drops) are needed to drive the charge injection. These findings are critical to future experiments in which FETs based on two or more grains are used to explore the transport properties of individual grain boundaries.

Experimental Method

Materials and Transistor Preparation. 6T, Au, Cr, Al, and single-crystal p-doped Si wafers were prepared or purchased in a manner similar to that described in ref 3b. 6T FETs were also fabricated as described in ref 3b, except for the chip cleaning process. Before deposition of 6T, each chip was cleaned by sonication in acetone for 15 min followed by exposure to O_2 plasma for 10 min at 250 mTorr and 200 W (four cycles). For the thiol-modified electrodes, the cleaned chips were submersed in a ~1 mM solution of dodecanethiol ($C_{12}H_{26}S$) in ethanol for at least 20 h to ensure full coverage of the gold electrodes with a self-assembled monolayer (SAM). Sexithiophene was subsequently deposited via vacuum deposition.

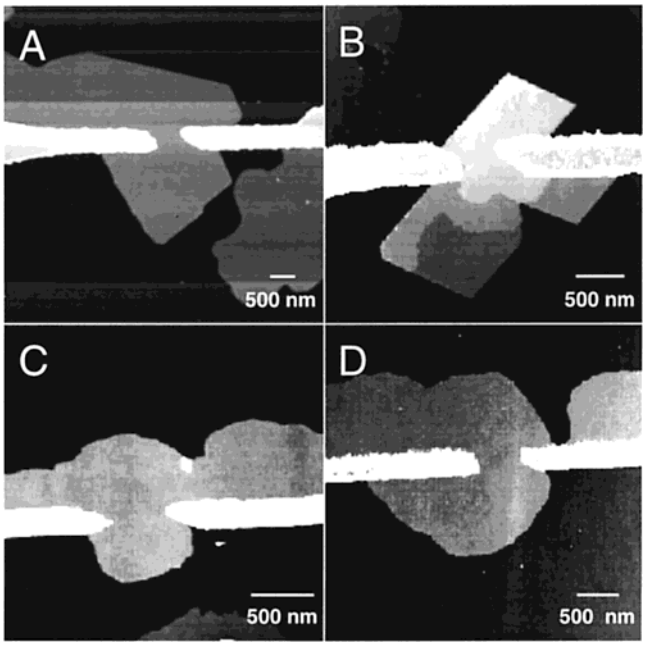

Figure 1. AFM height images of representative 6T FET structures. The 6T crystals shown are 5−14 nm tall and bridge the gaps between Au electrodes, which are 15−20 nm tall. The Au and 6T lie on 150 nm thick SiO_2; heavily doped Si underneath the SiO_2 serves as the gate.

Current−Voltage Measurements. Drain and gate voltages were applied with a Keithley 236 source measure unit and Keithley 6517A electrometer, respectively. The 236 also monitored current through the drain electrode and the 6517 monitored current through the source electrode. Both Keithleys shared a common ground, and the input impedance of each unit was 10^{14} Ω. Current−voltage measurements were performed under vacuum in a cryostat at ~10^{-6} Torr. Chips were mounted on the cryostat coldfinger and electrically contacted by spring-loaded pins.[10]

Temperature Experiments. Temperature was controlled from 5 to 300 K for the experiments performed under vacuum by pumping liquid helium into the copper cryostat coldfinger. The temperature of the coldfinger was monitored using a silicon diode sensor coupled to a Lake Shore L-330 controller.

Results

Figure 1 shows typical 6T FET structures fabricated in our lab. Figure 2 displays representative sets of $I_D - V_D$ characteristics at 300 and 5 K. The magnitudes of the currents shown in Figure 2 are typical for our devices. The device electrodes (Cr/Au ~1.5/15 nm) are pre-patterned on the SiO_2 surface (~150 nm thick) via electron beam lithography before 6T is vacuum deposited onto the substrate. Other details can be found in ref 3b.

Contact Area Dependence. Figure 3 shows log-linear plots of current through two different devices when the source and drain electrodes are switched. The device in Figure 3A is physically symmetric; that is, contact area with the 6T is the same for both electrodes. In Figure 3B, contact area with the 6T is not the same for both electrodes, that is, the device is

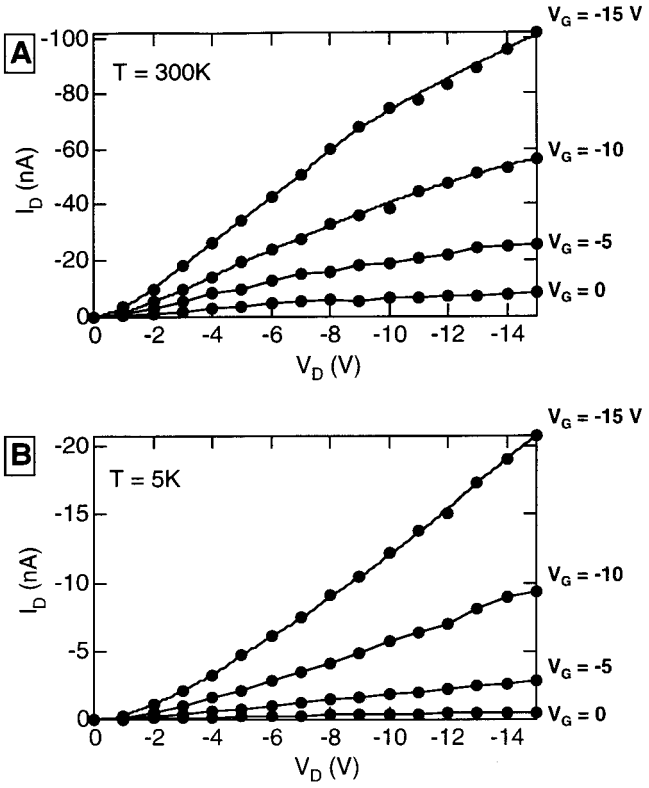

Figure 2. I_D-V_D characteristics of a typical 6T grain FET structure at room temperature (A) and 5K (B). The 6T in the device was 5 nm (2 molecular layers) tall.

physically asymmetric. As illustrated in the plot below Figure 3A, current through the device when electrode I is at ground (i.e., is the source) and II is biased negatively (i.e., is the drain) is nearly identical to the current through the device when II is at ground and I is biased negatively. In contrast, current through the asymmetric Figure 3B device is not the same when the two electrodes are switched; that is, hole transport from electrode I to II is not the same as that from II to I. However, when the contact area between II and the 6T is normalized with respect to the contact area between I and the 6T, the $I-V$ characteristics are nearly identical. Similar contact area dependence was observed in many devices. Contact area was determined from section analyses of the atomic force microscopy (AFM) height images to measure the Au/6T contact perimeter and 6T crystal height. These results are unambiguous evidence that the devices are contact limited. Furthermore, we see that transport through the devices is limited by the Au/6T contact area of the hole-injecting electrode, as more current is obtained from the Figure 2B device when electrode II is the source.

Temperature Dependence. Figure 4A shows an Arrhenius plot of I_D; the data were taken at $V_G = -15$ V and $V_D = -1$ V. The data correspond to the same device as that of Figure 2. At least two regimes are apparent in Figure 4A, one activated ($T \approx 150-300$ K) and one relatively inactivated ($T < 150$ K). An activation energy, or effective barrier Φ (see eq 6), of ~40 meV was determined from the slope of the thermally activated region. Plots of Φ versus V_D were obtained by constructing the Arrhenius plots at several different drain biases and constant V_G (Figure 4B). The same type of analysis was done to determine Φ as a function of V_G at constant V_D (Figure 4C).

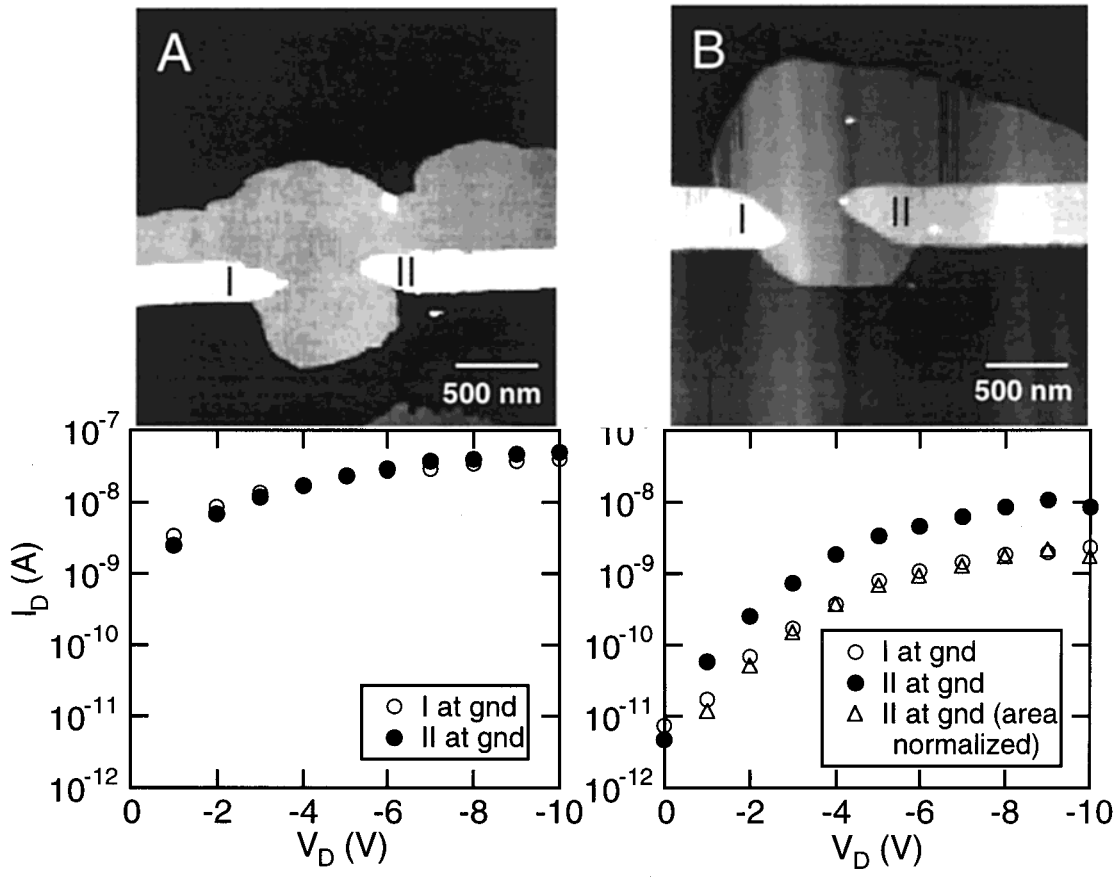

Figure 3. AFM height images of two different 6T devices with corresponding transport characteristics at $V_G = -10$ V. The 6T crystal is ~5 nm tall (2 molecular layers) in (A) and 12 nm tall (5 molecular layers) in (B). In the I_D-V_D plot for (B), the contact area between the 6T and electrode II (6T-II) was normalized (△) by dividing the area by the 6T−I contact area.

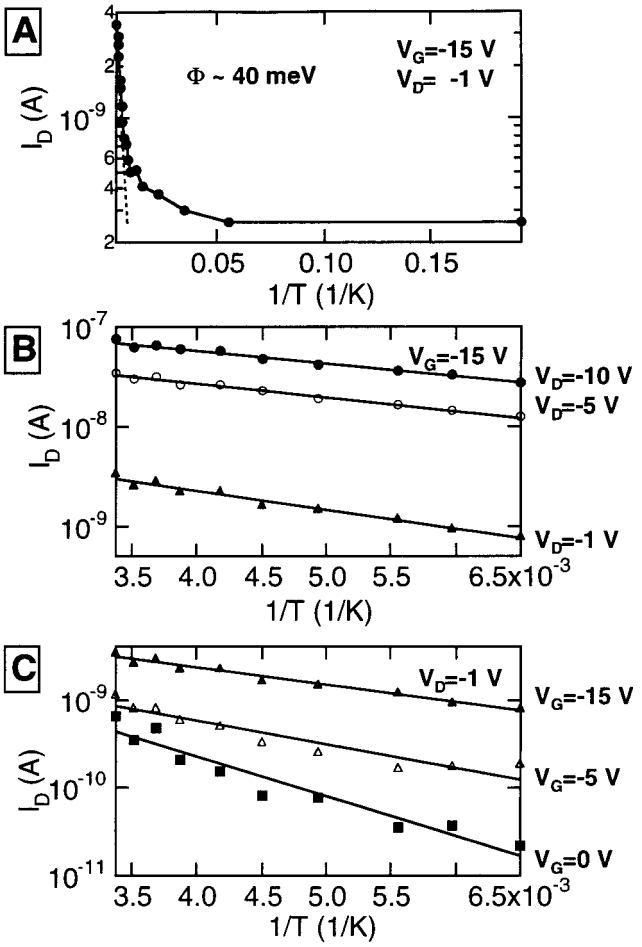

Figure 4. (A) Arrhenius plot of current at $V_G = -15$ V and $V_D = -1$ V for the device corresponding to Figure 2. An activation energy, or effective barrier Φ according to our model (eq 6), of ~40 meV is extracted from the thermally activated regime ($T > 150$ K). (B) Arrhenius plots of current in the activated regime at $V_G = -15$ V for $V_D = -10$, -5, and -1 V. (C) Arrhenius plots of current in the activated regime at $V_D = -1$ V for $V_G = -15$, -5, and 0 V.

The $\Phi - V_D$ and $\Phi - V_G$ graphs are shown in Figure 5. Similar plots were constructed to determine V_D and V_G dependences of the barrier according to the thermionic emission model (not shown).[11]

Fitting of Data to Models. Figure 6A shows an experimental $I_D - V_D$ trace at $V_G = -15$ V; superimposed are fits to the data according to the thermionic emission and drift/diffusion models (eqs 2A and 6, respectively). There are two traces for the drift/diffusion model, one with a constant mobility μ_o and one with a field-dependent mobility. All fits utilized adjustable parameters in addition to the effective barrier determined from the temperature studies. For the drift/diffusion model (eq 6), the adjustable parameters included μ_o, the power law exponent m, and the threshold voltage V_T.[12] For the thermionic emission model, the adjustable parameter was v_r. Clearly, the drift/diffusion model with either constant or field-dependent mobility gives a much better fit to the experimental data than the thermionic emission model. Figure 6B shows that the drift/diffusion model gives good fits for the $I_D - V_D$ characteristics over the range of gate voltages employed in this study. In Figure 6B, $\mu_o = 10^{-4}$ cm^2/Vs, $m = 0.2$, $V_T = 8$ V, $n = 1.1$, and $V_{Do} = -1$ V. The close fit between the data and the drift/diffusion model with field-dependent mobility suggests that this mechanism is the one by which holes are injected from the Au into the 6T.

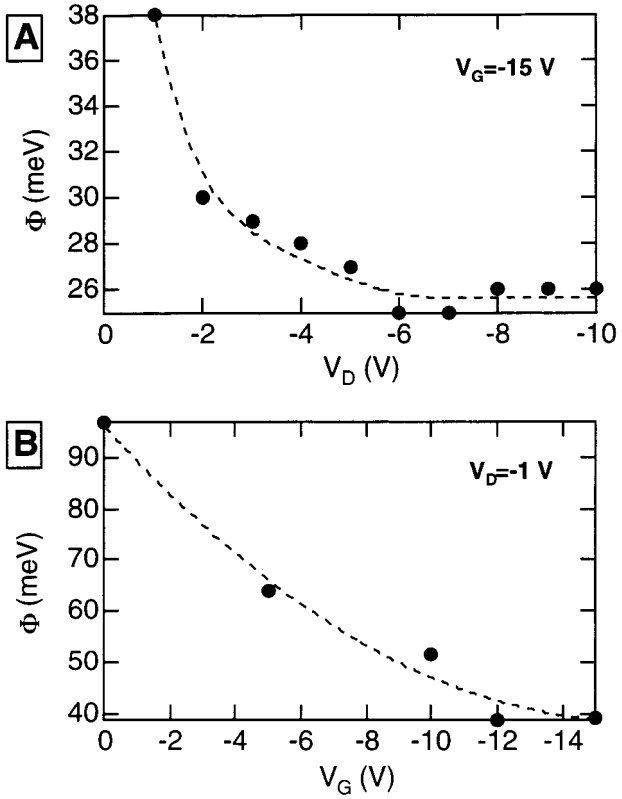

Figure 5. (A) Φ versus V_D at $V_G = -15$ V from Arrhenius plots of I_D at $V_G = -15$ V (see Figure 4B). (B) Φ versus V_G at $V_D = -1$ V from Arrhenius plots of I_D at $V_D = -1$ V (see Figure 4C).

Contact Resistance Estimation. Overall device resistance can be determined as a function of V_D and V_G using the $I_D - V_D$ characteristics. Resistance is defined as

$$R = \frac{\partial V_D}{\partial I_D}\Big|_{V_G} \tag{7}$$

Figure 7 shows the resistance R as a function of V_D for $V_G = -15$ V (Figure 7A) and as a function of V_G for $V_D = -1$ V (Figure 7B). Because the device is [source] contact limited over the range of bias applied, the device resistance is equal to the contact resistance. Figure 7 indicates that the contact resistance is sensitive to both the transverse gate field and the lateral field.

Thiol Modified, Cr, and Al Electrodes. Using thiol adsorption chemistry,[13] we fabricated 6T FET structures in which the surfaces of the Au electrodes were modified with a self-assembled monolayer of $C_{12}H_{26}S$. Figure 8A shows measured $I_D - V_D$ characteristics for a device in which a SAM of the dodecanethiol was formed on the Au electrodes before 6T was vacuum deposited. Transport was clearly inhibited by the presence of the SAM. We also fabricated devices using Cr and Al electrodes instead of Au. The $I_D - V_D$ characteristics for the Cr devices were similar to those for the thiol modified electrode devices (Figure 8B). The Al devices, however, did not turn on, most likely because of formation of an oxide layer around the Al electrodes.

Discussion

The key result of this work is that hole transport through 6T single-grain FETs such as those shown in Figure 1 is injection limited. This conclusion was arrived at by observation of the source/6T contact area dependence of current, as demonstrated

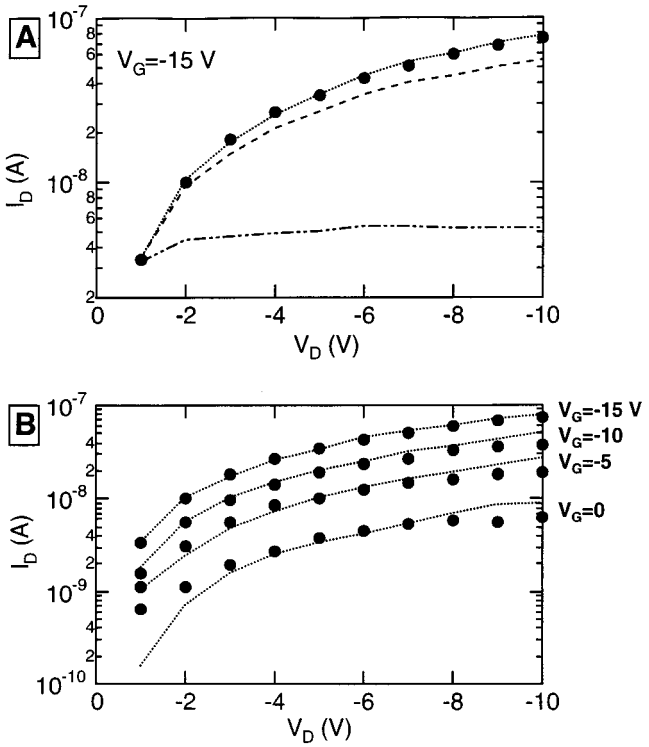

Figure 6. (A) I_D-V_D plot ($V_G = -15$ V) of experimental data (●) and simulated data based on the thermionic emission (−••), drift/diffusion with constant mobility (---), and drift/diffusion with field dependent mobility (•••) models. In the last case, the mobility was modeled as $\mu = \mu_o(V_D/V_{Do})^{0.2}$ for $V_D > V_{Do}$, where $V_{Do} = -1$ V and μ_o is the corresponding mobility. The experimental data are from the same device as that of Figures 2, 4, and 5. (B) Experimental (●) and simulated (•••) data from the drift/diffusion model with field dependent mobility (as in (A)).

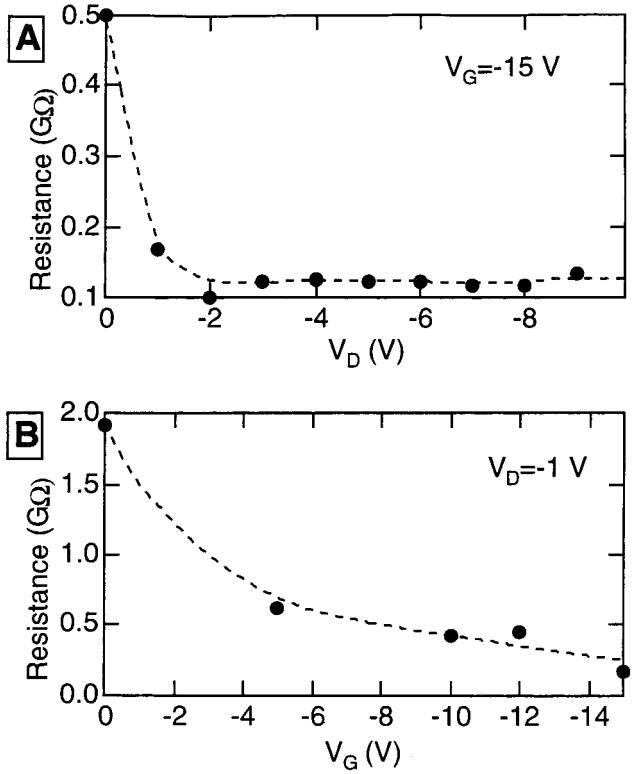

Figure 7. Drain (A) and gate (B) voltage dependences of the overall device resistance from Figure 2A and eq 7. The device resistance equals the contact resistance because the device is source contact limited.

in Figure 3. The data show that the source/6T contact is the principal bottleneck to charge transport in these devices.[14] We attribute this bottleneck to a combination of an intrinsic hole injection barrier, a region of molecular disorder around the electrode, and simply the small contact area between the electrode and the grain. Based on the work function of Au and the ionization potential of 6T, one predicts a hole injection barrier of ∼0.1 eV (Schottky−Mott limit). This prediction does not include contact effects that can increase the barrier, for example, charge transfer at the interface resulting in an interface dipole.[15] Although detailed studies of Au/6T interfaces are lacking in the literature, it seems reasonable that a hole injection barrier at the source/6T interface exists, especially because the 6T in our devices is deposited *after* deposition of the Au electrodes (a top contact FET may not be limited by an injection barrier because of penetration of the metal atoms into the soft organic).[15a,b] Molecular disorder near the contacts is also likely because the 6T appears to grow conformally to the Au electrodes, which have rough edges that should inhibit crystalline perfection around the electrode perimeters. Finally, because the electrodes only touch the 6T grains around their perimeters, the total electrode contact area (∼10^4 nm^2) is exceedingly small, which makes the electrical behavior of the contacts more pronounced. Thus, there are clear reasons why the source/6T contact limits transport through the 6T grain device.

We modeled the FETs as a pair of back-to-back Schottky diodes (Chart 1B) based on the observation that the devices were limited by the hole-injecting contact. The current limiting nature of the source/6T diode arises naturally because this junction is reverse biased and therefore more resistive than the forward-biased drain/6T junction. Our fits of experimental data to diode models therefore only required consideration of the reverse-bias current.

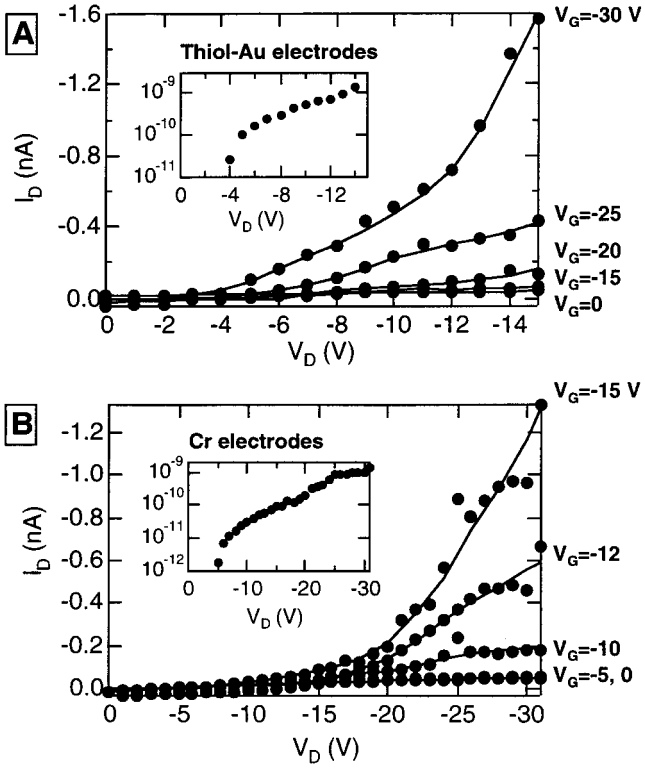

Figure 8. (A) I_D-V_D characteristics of a 6T device in which a SAM of dodecanethiol was formed on the Au electrode before deposition of 6T. A log−linear plot is shown in the inset for $V_G = -30$ V. (B) I_D-V_D characteristics of a 6T device with Cr electrodes. A log-linear plot is shown in the inset for $V_G = -15$ V.

The model that best fits the data is drift/diffusion with a field-dependent mobility (Figure 6). We note that even with a constant mobility, the drift/diffusion model still provides a reasonable fit. The drift/diffusion model offers a better fit to the experimental data than the thermionic emission model because of the explicit field dependence in the preexponential term (eq 6). This explicit field dependence is absent in the preexponential term of the thermionic emission model (eq 2A). The thermionic emission model does allow for field-dependent barrier lowering. However, although barrier lowering is observed in our devices (Figure 5), it is not sufficient to explain the field dependence of the current. This outcome has also been observed in Ni Schottky contacts to hydrogenated amorphous silicon.[16]

The fact that the source/6T contact is limiting means that the voltage drop, and hence electric field, at this interface is large. This conclusion is supported by data from recent potentiometry experiments that indicate that the potential gradient in 6T is not uniform across the gap but is greatest within 100 nm of the hole-injecting electrode.[14] In other words, the characteristic length l describing the electric field is not the entire length of the channel but rather only a fraction of the channel. Because $V_{Do} = -1$ V,[12] $l \approx 100$ nm gives $E_{Do} \approx 10^5$ V/cm. This field estimation is consistent with the results from previously reported work that indicate that hole mobilities in organic films become field dependent at fields $>10^5$ V/cm.[8] We also estimated from the fits in Figure 6 the carrier mobility μ_o through the depletion region near the source electrode. Our value for μ_o, 10^{-4} cm^2/Vs, is low compared with the highest reported mobilities for 6T films.[4] However, a low μ_o is expected because the region around the hole-injecting electrode is likely to be disordered (Chart 1C).

The value of Φ we obtained at small V_D and V_G (Figure 5B) approaches the 0.1 eV Schottky−Mott limit for a Au/6T junction. Although Φ may be low, we consistently observe source-contact-limited behavior in our devices. This result indicates that there must be an intrinsic barrier (ϕ_B) associated with the source/6T junction. Our low values of Φ, which we have defined as an effective barrier, are most likely the combined result of hole trapping and field-induced barrier lowering.

The I_D-V_D characteristics for our 6T devices clearly show a gate voltage dependence. The gate effect in our devices is reflected in both the V_G dependence of the effective barrier Φ and the explicit V_G dependence of the electric field in the preexponential term. Application of a negative gate voltage increases the number of holes p in the 6T due to capacitive coupling.[17] However, in contrast to conventional Si FETs, the sensitivity of the $I-V$ characteristics to the gate voltage in our devices is due to modulation of the source/6T contact behavior and not the change in resistivity of the 6T grain. The increased hole concentration increases the interfacial electric field at the source/6T contact (Chart 2B) and decreases the concentration of empty traps in the disordered region near the contact. Effectively, our devices are analogous to previously reported Schottky contact Si FETs in which the gate field modulates the charge injection barrier at the source contact.[18]

The high contact resistance associated with our 6T grain devices is due to the reasons already discussed in detail and not to "dirty" electrodes.[19] If the electrodes were unclean (e.g., not free of resist remnants), then changing the contacts would not have a dramatic effect on the $I-V$ characteristics. Results from the thiol-modified Au devices (Figure 8A) and the devices employing Cr electrodes instead of Au (Figure 8B) illustrate dramatic effects on the $I-V$ characteristics. This result confirms that we do have control over the quality of the contacts and that the contacts play an important role in our devices. Figure 7 also illustrates that the contact resistance is a function of both drain and gate voltages. This result is expected because the injecting Au/6T interface is Schottky-like, and both V_D and V_G influence the field in the contact region.

In summary, we have demonstrated that the device characteristics of 6T grain FETs, such as those in Figure 1, reflect the properties of the hole-injecting contact, which behaves as a reverse-biased diode. Through activation energy measurements and device modeling, we have determined that the transport mechanism that best describes hole injection from the source electrode into the semiconductor is a drift/diffusion process with a field dependent mobility $\mu = \mu_o(V_D/V_{Do})^{0.2}$, where $E_{D0} \sim 10^5$ V/cm and $\mu_o \sim 10^{-4}$ cm^2/Vs. The contact resistance is large in our devices, on the order of 10^9 Ω for a typical ~300-nm wide electrode. We have demonstrated the ability to modify the Au/6T contacts using thiol adsorption chemistry (Figure 8A). The particular thiol we chose made the contacts worse. However, based on recently reported work[20] we believe that the contacts can be improved by utilizing a thiol with an appropriate dipole.

The larger implication of this work is that contacts cannot be ignored for devices based on individual grains of organic semiconductors. Contact resistance is large in these devices and can only be neglected if the resistance of the semiconductor is significantly greater than the resistance of the metal/semiconductor contact. The presence of a grain boundary in the active channel exemplifies such an overriding resistance.[2c] Full characterization of transport through a single grain boundary would contribute to the understanding of organic thin film transistors, which have been proposed for numerous applications including smart cards and backplanes for flat-panel displays,[21] because grain boundaries influence, if not dominate, total device behavior of organic TFTs.[2] Our FET structure is particularly well suited for such grain boundary experiments because the experimental conditions can be manipulated to increase the probability of grain boundary growth between the source and drain electrodes. The results from the present study are thus crucial to future experiments in which FETs based on two or more grains are used to probe the transport characteristics of grain boundaries in organic semiconductors.

Acknowledgment. This work was supported by the David and Lucile Packard Foundation and by the National Science Foundation under DMR-9624154-001. A.B.C. acknowledges Prof. Chris Palmstrom for helpful discussions.

References and Notes

(1) (a) Katz, H. E.; Bao, Z. *J. Phys. Chem. B.* **2000**, *104*(4), 671 (Review). (b) Klauk, H.; Gundlach, D. J.; Nichols, J. A.; Jackson, T. N. *IEEE Trans. Elec. Dev.* **1999**, *46*(6), 1258. (c) Gundlach, D. J.; Jackson, T. N.; Schlom, D. G.; Nelson, S. F. *Appl. Phys. Lett.* **1999**, *74*, 3303. (d) Dimitrakopoulos, C. D.; Purushothaman, S.; Kymissis, J.; Callegari, A.; Shaw, J. M. *Science* **1999**, *283*, 822.

(2) (a) Horowitz, G.; Hajlaoui, M. *Adv. Mater.* **2000**, *12*(14), 1046. (b) Schön, J. H.; Batlogg, B. *Appl. Phys. Lett.* **1999**, *74*(2), 260. (c) Kelley, T. W.; Frisbie, C. D. *J. Phys. Chem. B*, submitted for publication.

(3) (a) Chwang, A. B.; Granstrom, E.; Frisbie, C. D. *Adv. Mater.* **2000**, *12*(4), 285. (b) Granstrom, E.; Frisbie, C. D. *J. Phys. Chem. B* **1999**, *103*, 8842.

(4) (a) Horowitz, G.; Hajlaoui, M.; Hajlaoui, R. *J. Appl. Phys.* **2000**, *87*(9), 4456. (b) Torsi, L.; Dodabalapur, A.; Rothberg, L. J.; Fung, A. W. P.; Katz, H. E. *Phys. Rev. B* **1998**, *57*, 2271. (c) Schön, J. H.; Kloc, Ch.; Laudise, R. A.; Batlogg, B. *Phys. Rev. B* **1998**, *58*, 952. (d) Lovinger, A. J.; Rothberg, L. J. *J. Mater. Res.* **1996**, *11*, 1581 (Review). (e) Garnier, F.; Horowitz, G.; Peng, X.; Fichou, D. *Adv. Mater.* **1990**, *2*(12), 592.

(5) (a) Sze, S. M. *Physics of Semiconductor Devices*, 2nd ed.; John Wiley & Sons: New York, 1981, Ch. 5. (b) Rideout, V. L. *Thin Solid Films* **1978**, *48*, 261.

(6) Fujimoto, H.; Nagashima, U.; Inokuchi, H.; Seki, K.; Cao, Y.; Nakahara, H.; Nakayama, J.; Hoshino, M.; Fukuda, K. *J. Chem. Phys*. **1990**, *92*, 4077.

(7) Because the disorder is present at both the hole-injecting (source) and hole-receiving (drain) contacts, there is naturally a contact resistance associated with each of the Au/6T contacts. However, because of the energy band offsets, the contact resistance at the reverse-biased hole injecting contact is always higher.

(8) (a) Dodabalapur, A.; Torsi, L.; Katz, H. E. *Science* **1995**, *268*, 270. (b) Torsi, L.; Dodabalapur, A.; Katz, H. E. *J. Appl. Phys*. **1995**, *78*(2), 1088. (c) Abkowitz, M.; Facci, J. S.; Stolka, M. *Chem. Phys*. **1993**, *177*, 783.

(9) Implicit in the T^0 dependence of the preexponential is a $T^{3/2}$ dependence of N_V (assuming a parabolic density of states function) and a $T^{-3/2}$ dependence of the carrier mobility μ (due to phonon and impurity scattering). We do not know a priori what the density of states function looks like for 6T grains only a few molecules in thickness, so we do not know the exact temperature dependence of N_v. However, for the purpose of analysis we will assume that the temperature dependences just noted hold (see note 11).

(10) The transistors were electrically isolated from the coldfinger by a small (1 cm^2) square of [thermally conductive] sapphire.

(11) For the thermionic emission model, the temperature dependence of the preexponential in eq 2A was taken to be T^2. The T^2 dependence arises from a $T^{3/2}$ dependence of N_V (assuming a parabolic density of states function) and a $T^{1/2}$ dependence of the recombination velocity, v_r. The barrier was therefore determined from Arrhenius plots of I_D/T^2 (Richardson plots). In assessing the validity of the temperature dependence assumptions for both thermionic emission and drift/diffusion, we looked at various temperature dependences and corresponding Arrhenius plots. The magnitude of the barrier changed with the temperature dependence, but this did not affect which model best fit the experimental data.

(12) The exponent n was determined from log−log plots of $(I_D/\exp(-\Phi/kT))$ versus $(V_G - V_T)$ after V_T was chosen. V_{Do} was determined as the drain voltage at which the drift/diffusion with constant mobility trace began to deviate from the experimental data. $N_v \sim 10^{21}$ cm^{-3}, which is the density of 6T molecules.

(13) For a review of thiol adsorption chemistry, see (a) Andres, R. P.; Datta, S.; Janes, D. B.; Kubiak, C. P.; Reifenbergr, R. *The Handbook of Nanostructured Materials and Nanotechnology*, Nalwa, H. S., Ed.; Academic Press: New York, 1998. (b) Dubois, L. H.; Nuzzo, R. G. *Annu. Rev. Phys. Chem*. **1992**, *43*, 437. (c) Bain, C. D.; Whitesides, G. M. *Adv. Mater*. **1989**, *28*(4), 506.

(14) This has been confirmed by potentiometry experiments in which potential drops at various points between the source and drain electrodes of a 6T grain FET were measured using a conducting AFM probe (Seshadri, K.; Frisbie, C. D. submitted for publication in *Appl. Phys. Lett*.

(15) Recent ultraviolet photoelectron spectroscopy studies of metal/organic semiconductor interfaces have shown significant deviations of $(E_{HOMO} - E_F)$ from Schottky−Mott limits. See, for example, (a) Hill, I. G.; Rajagopal, A.; Kahn, A.; Hu, Y. *Appl. Phys. Lett*. **1998**, *73*(5), 662. (b) Rajagopal, A.; Kahn, A. *J. Appl. Phys*. **1998**, *84*(1), 355. (c) Kendrik, C.; Semancik, S. *J. Vac. Sci. Technol. A* **1998**, *16*, 3068.

(16) Heller, D. E.; Dawson, R. M.; Malone, C. T.; Nag, S.; Wronski, C. R. *J. Appl. Phys*. **1992**, *72*(6), 2377.

(17) In conventional silicon p-FETs, the holes originate from the bulk silicon so that a conductive accumulation layer results when sufficiently negative voltages are applied. In our devices, there is no "bulk" 6T in the same sense as the silicon FET because the 6T crystals are only 1−6 molecular layers tall. The holes come from the source electrode.

(18) Lepselter, M. P.; Sze, S. M. *Proc. IEEE* **1968**, *56*, 1400.

(19) We can compute a normalized contact resistance by multiplying R (10^9 Ω) by the perimeter of the Au/6T contact ($\sim 10^{-4}$ cm). Thus, we find a normalized contact resistance of $\sim 10^5$ Ω-cm, which is comparable to the normalized contact resistance associated with 6T film devices. See (a) Lin, Y. Y.; Gundlach, D. J.; Jackson, T. N. *MRS Symp. Proc*. **1996**, *413* and (b) Horowitz, G.; Hajilaoui, R.; Fichou, D.; El Kassmi, A. *J. Appl. Phys*. **1999**, *85*(6), 3202.

(20) (a) Campbell, I. H.; Kress, J. D.; Martin, R. L.; Smith, D. L.; Barashkov, N. N.; Ferraris, J. P. *Appl. Phys. Lett*. **1997**, *71*(24), 3528. (b) Campbell, I. H.; Rubin, S.; Zawodzinski, T. A.; Kress, J. D.; Martin, R. L.; Smith, D. L. *Phys. Rev. B* **1996**, *54*(20), 14321.

(21) (a) Crone, B.; Dodabalapur, A.; Lin, Y. Y.; Filas, R. W.; Bao, Z.; LaDuca, A.; Sarpeshkar, R.; Katz, H. E.; Li, W. *Nature* **2000**, *403*(6769), 521. (b) Lin, Y.Y.; Dodabalapur, A.; Sarpeshkar, R.; Bao, Z.; Li, W.; Baldwin, K.; Raju, V. R.; Katz, H. E. *Appl. Phys. Lett*. **1999**, *74*(18), 2714. (c) Jackson, T. N.; Lin, Y. Y.; Gundlach, D. J.; Klauk, H. *IEEE J. Sel. Topics. Quantum Elec*. **1998**, *4*(1), 100.